Proceedings of the ASME 2010 Pressure Vessels & Piping Division / K-PVP Conference
PVP2010
July 18-22, 2010, Bellevue, Washington, USA

PVP2010-25989

DYNAMICS OF CAVITATING FLOW AND FLEXURAL WAVES IN FLUID-FILLED TUBES SUBJECT TO AXIAL IMPACT

Kazuaki Inaba*and Joseph E. Shepherd
Department of Mechanical Sciences and Engineering
Graduate School of Science and Engineering
Tokyo Institute of Technology
2-12-1 I6-5, Ookayama, Meguro-ku, Tokyo 152-8550, Japan
Email: inaba@mech.titech.ac.jp

ABSTRACT

We have experimentally studied the coupling of flexural waves in water-filled tubes with cavitating flow. To examine the cavitation events in the tube, we used a transparent polycarbonate (PC) tube. The flexural waves are generated by stress waves in the water propagating along the tube axis. A steel impactor is accelerated by gravity and strikes a polycarbonate buffer placed on top of the water surface within the tube. Strain gages measure hoop strain along the polycarbonate tube and a piezoelectric pressure gage measures the pressure at the bottom of the tube. The events were visualized by a high-speed video camera synchronized with the strain and pressure measurements. The impact of the projectile creates a stress wave propagating along the tube and coupled to the pressure wave in water. A sequence of traveling waves results and when the pressure in the waves drops below the vapor pressure, cavitation occurs in the tube. When cavitation bubbles are present, the tube vibrates at the natural frequency of the second mode of the circular ring. The duration of the cavitation can be estimated from a balance between the buffer kinetic energy and the work done in accelerating the fluid. Cavitation does not occur uniformly or simultaneously; cavitation events are observed near the bottom surface of the buffer, the middle of the tube, and at the bottom (closed) end. High-speed video of the cavitation events reveals that the cavities are clusters of bubbles that have a rosary or grape-bunch appearance.

NOMENCLATURE

- A Area of tube cross section, $2\pi Rh$
- a_f sound speed in fluid (water), 1488 m/s
- c Korteweg wave speed
- c_b bar wave speed in solid $\sqrt{E/\rho_s}$
- u Velocity
- E Young's modulus of tube material, polycarbonate 2.4 GPa
- ν Poisson ratio of tube material, $\sim$0.3
- f Natural frequency of a circular ring
- h Thickness of tube wall
- I Tube cross section, moment of inertia, $2\pi Rh^3/12$
- K Bulk modulus of water, 2.2 GPa
- L Length of tube
- n nth mode (order)
- R Average of inner and outer radius of tube
- V_B Buffer velocity immediately after impact
- V_P Projectile impact velocity
- β FSI coupling parameter, $K2R/(Eh)$
- ρ_s Density of tubular structure (polycarbonate), 1250 kg/m^3

*Address all correspondence to this author.

ρ_f Density of fluid (water), 1000 kg/m^3

INTRODUCTION

An example of fluid-structure interaction (FSI) that is very relevant to industrial fluid distribution systems is water hammer [1–3]. Water hammer is the consequence of rapid flow changes due to valve or pump operation in a fluid-filled piping system. The effects are manifested as propagating waves of water pressure and piping mechanical stress waves that are coupled by forces and motion occurring at the fluid-structure boundary, i.e., the pipe interior surface. If the propagating waves result in low or negative pressures within the fluid, cavitation, which is the generation of low-pressure gas bubbles, will occur within the water. These bubbles significantly influence the dynamics of the wave propagation in the water.

Water hammer resulting in substantial cavitation is known as "column separation" [4] since the cavitation often results in the fracture of the fluid column into parts separated by large gas bubbles. The collapse of the gas bubbles results in rapid pressure rises that create severe mechanical loads on pipelines and supporting structures. Due to the industrial importance of this topic, there is a substantial engineering literature, reviewed by Bergant et al. [4]. Recent work from the group of Tijsseling [5–7] has reported cavitation experiments with steel tubes with various configurations such as a closed pipe, a pipe with an elbow, and a pipe with a tee branch.

In this paper, we report some observations about FSI and cavitation that are relevant to the analysis of water hammer in a very flexible piping system. In order to focus on the fundamental aspects of FSI and water hammer, we have used a very simple experimental test setup with projectile impact creating propagating waves in water-filled tubes as shown in Fig. 1. This configuration has been used by many other researchers to examine diverse issues such as cavitation [8], metal forming [9], and underwater shock wave simulations [10, 11].

As discussed by Shepherd and Inaba [12], the extent of fluid-solid coupling in this geometry is determined by the parameter $\beta = K2R/(Eh)$. Unlike the case of normal impact of a shock wave, the coupling depends only on material properties and is independent of flow behind the shock. In the simplest analysis, the fluid in the tube is treated as compressible and the motions in the fluid are treated as quasi-one dimensional. Balancing the acoustic pressure in the fluid with static membrane stress of the tube, the FSI flexural waves are predicted to propagate with the

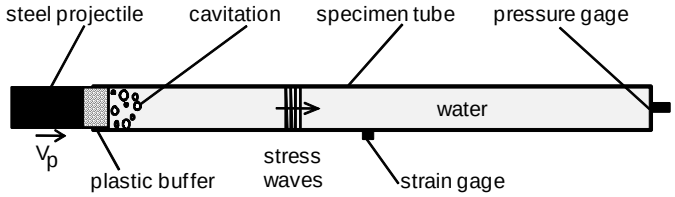

Figure 1. Schematic diagram of axi-symmetric water-in-tube configuration for generation of shell flexural waves coupled with stress waves propagating in water.

Korteweg speed

$$c = \frac{a_f}{\sqrt{1+\beta}} \,. \tag{1}$$

The limitations of this analysis and extensive comparisons with test results are given in the literature on water hammer [1–3]. Shepherd and Inaba [12] found that the primary flexural wave speed in the present test configuration could be predicted by Eq. 1 with reasonable accuracy for both metal and polymer tubes.

In the present experiments, β = 6.36 or 12.5, whereas in commercial steel pipe, a value of $0.1 \leq \beta \leq 0.4$ is typical. As a consequence of the large values of β, the Korteweg speeds in the present experiment are predicted (and observed) to be substantially lower (see Table 1) than the water sound speed.

EXPERIMENTAL SETUP

Free Fall Impact Tester

Our free-fall impact tester consists of a guide tube and a test specimen as shown in Fig. 2. The guide tube with a diameter of 50 mm is mounted vertically above the specimen, a polycarbonate tube filled with water. The 1.5 kg steel projectile is accelerated by gravity from a height of 2.2 m. The projectile is not completely ejected from the guide tube when it impacts a polycarbonate buffer placed on the water surface. A gland seal is used to prevent water moving through the clearance space between the buffer and tube. In this fashion, the stress waves due to the impact of the projectile are transmitted directly to the water surface inside the specimen tube.

The impact-generated pressure waves in the water create stress waves and deformation in the tube, and the resulting coupled fluid-solid motion propagates downward from the buffer toward the bottom of the tube. The deformation of the tube is measured by strain gages oriented in the hoop and longitudinal

directions, and the pressure in the water is measured by a piezoelectric transducer mounted in an aluminum fitting sealed to the bottom of the tube. The bottom of the tube is fastened to an aluminum bar mounted in a lathe chuck that is placed directly on the floor.

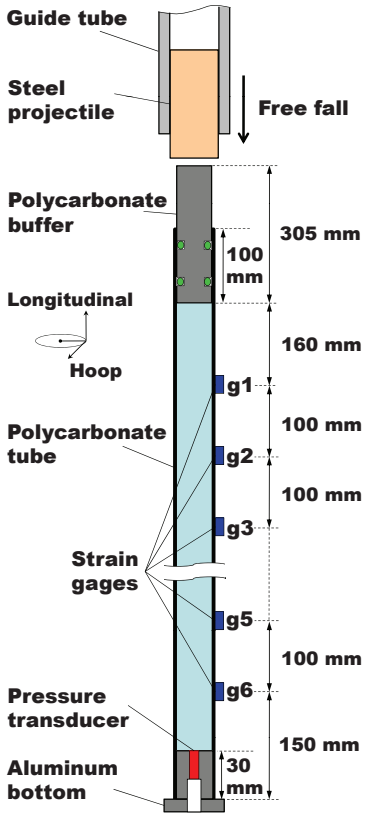

Figure 2. Test specimen tube, #3, with projectile, buffer, pressure transducer, and strain gages. Test specimen tube, #2, used a shorter buffer (100 mm) and was without strain gages for visual observations.

Test Conditions and Specimens

Dimensions of polycarbonate specimen tubes are summarized in Table 1. The radius given in the table is the average of the inner and outer values. For tube #3, the outer diameter was 50.5 mm and inner diameter 37.8 mm; for tube #2, the outer diameter was 42 mm O.D. and inner diameter 38.2 mm. The lengths of the water-filled section in tests with the tube #3 and #2 are 0.72 m and 0.82 m, respectively.

Table 1. Test Matrix.

Shot	Tube	L [m]	h [mm]	R [mm]	β	c [m/s]
57-63	#3	0.910	6.39	22.1	6.36	548
66-77	#2	0.904	3.08	21.0	12.5	404

Strain gages were mounted in the hoop and longitudinal directions at 100 mm increments for tube #3 (see Fig. 2). A high-speed video camera (Vision Research Phantom v7.3) is used to observe buffer motions in shots 57-60, 63, 68 and cavitation phenomena in shots 61, 62, 69-77. The buffer speed just after the impact is computed from a frame-by-frame analysis of the video recording. The typical projectile speed just before the impact is V_P = 6.4 $\pm$ 0.1 m/s and the typical buffer speed just after the impact is V_B = 5.3 $\pm$ 0.1 m/s. The projectile speed is in good agreement with estimated speed of 6.42 m/s for free fall from 2.1 m height. In previous studies [12], we confirmed that fluid pressure observed in the tube is close to the pressure estimated with the acoustic relationship

$$\Delta p = \rho_f \, c \, \Delta u \, , \tag{2}$$

where c is the water hammer (Korteweg) speed (estimated by Eqn. 1) and Δu is the change in velocity of the fluid (water) estimated as the buffer velocity V_B. For tube # 3, the estimated peak pressure in the wave created by the initial buffer motion is about 2.9 MPa, which is consistent with the measured peak strain of 4 $\times$ 10^{-3} and static deformation of the tube.

RESULTS AND DISCUSSION

Fluid Structure Interaction

The impact of the projectile creates a stress wave propagating along the tube coupled to the pressure wave in the water. Figure 3 is a stacked perspective view of the hoop strain histories (black) measured at gages g1-g6 and pressure history (red) at the tube bottom. The origin of the time axis (0 ms) is selected as when the hoop strain at g1 becomes larger than a set threshold value. The origin of the distance axis is at the buffer bottom surface. The trajectory of the primary wave is shown as a straight blue line located at the leading edge of the strain wave signal. The extrapolation of the strain wave trajectory to the tube end shows that the pressure wave arrives at the same time as the

leading edge of the strain wave. In shots 57-63, the averaged primary wave speed is 555 $\pm$ 10 m/s, consistent with the nominal Korteweg speed of 548 m/s. The primary wave can be observed to propagate from the buffer to the tube end, reflects and propagate back to the buffer twice. After the second reflection from the buffer at 6 ms, the waves become less distinct but a disturbance can be observed to arrive at the bottom at 8 ms.

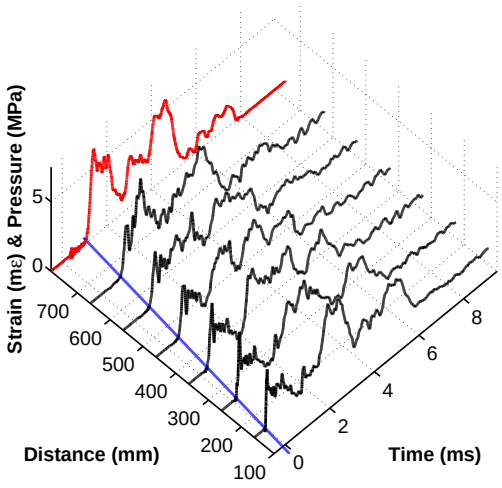

Figure 3. Hoop strain and pressure histories for shot 63, at early times: -0.5 $\leq t \leq$ 9.5 ms.

After 8 ms, the pressure and strain signals vanish until the sudden appearance of low-amplitude, rectangular loading pulse that emerges at 43 ms (see Fig. 4) from the bottom of the tube. This "reloading event" appears to be connected with the collapse of a cavitation region at the bottom of the tube. Similar events are seen in shots 60-63 but the timing and amplitude of the event vary in each shot.

Figure 5 shows the hoop and pressure histories during the period 40 to 55 ms when the reloading event occurs for shots 60 and 63. In these shots, we can observe small oscillations in strain prior to the onset of the reloading event at 40 ms. There is also a small compressive disturbance visible just prior to the onset of the reloading pulse. It appears that the weak compressive wave collapses the cavitation bubbles at the end of the tube to initiate the reloading event. The reloading event is then terminated by

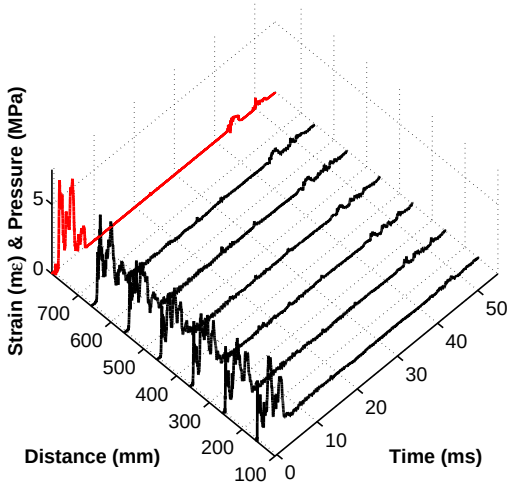

Figure 4. Hoop strain and pressure histories for shot 63 at long times: -0.5 $\leq t \leq$ 50 ms.

an expansion (rarefaction) wave originating from the reflection of reloading pulse from the buffer.

Vibrational Analysis

To examine the phenomena during the low pressure period between 8 and 40 ms, we have analyzed strain signals, Fig. 6, during this time to determine the frequency content, Fig. 7 with a Fast Fourier transform (FFT). The results for shots 60–62 are very similar to those for shot 63.

In Fig. 7, there are pronounced peaks in the spectrum for three frequency ranges: 1800-2300 Hz, 750-800 Hz, and $\sim$ 250-350 Hz. These frequencies are all substantially less than the *hoop frequency*

$$f_H = \frac{1}{2\pi R}\sqrt{\frac{E}{\rho(1-\nu^2)}} \tag{3}$$

of 10.5 kHz. The hoop frequency is a structural mode (no FSI considered) that corresponds to the breathing or axisymmetric radial motion of a tube section. The hoop motion is the largest contributor to the power spectrum in the vibration of detonation tubes [13], which have similar traveling load excitation. However, in the present experiments, the hoop mode is not observed

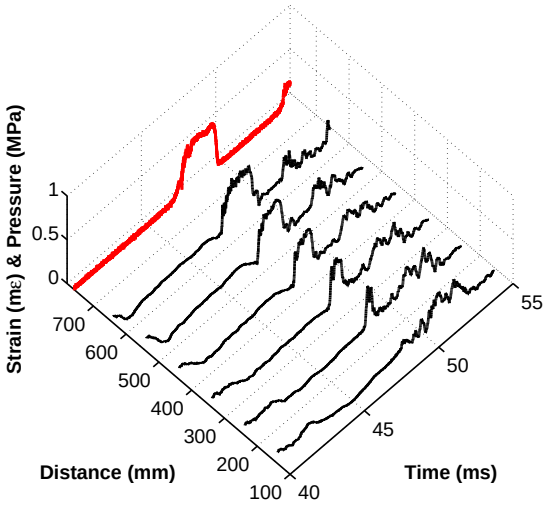

(a) shot 60

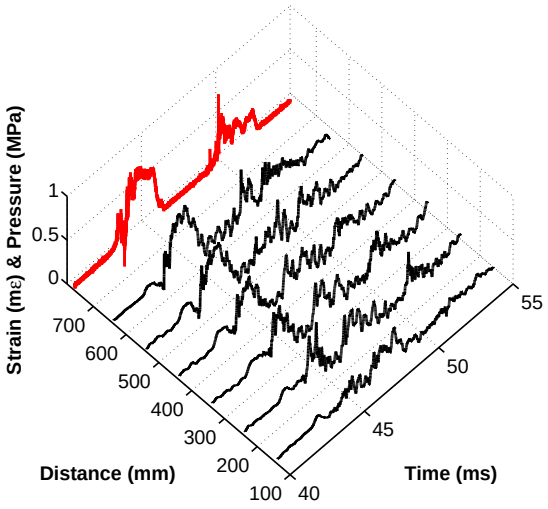

(b) shot 63

Figure 5. Hoop strain and pressure histories at the time of the reloading event, $40 \leq t \leq 55$ ms.

to participate strongly in the vibration induced by the impact or subsequent reloading events. In general, the amplitude of vibration of the tube wall and the pressure fluctuations are quite small during the dwell period between 8 and 10 ms.

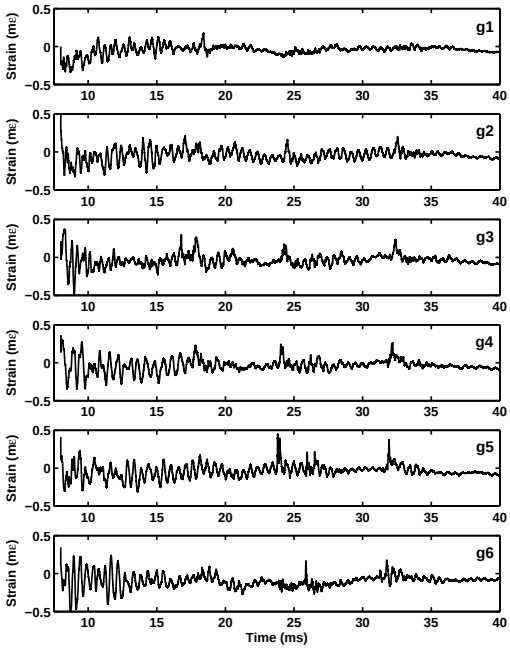

Figure 6. Hoop strain histories after the initial large-amplitude oscillations for shot 63.

There are several possible explanations for the frequency peaks that are observed in the spectrum. The theory of vibration of liquid-filled cylindrical shell [14–16] predicts a large number of modes with various shapes. At low-frequency only two axially symmetric modes are active, one corresponds to axial waves propagating with a phase speed approximately equal to the bar speed c_b in the shell material, the other is a coupled shell-fluid mode propagating with a phase speed approximately equal to the Korteweg phase speed c = 1452 m/s. The lowest order modes corresponding to axial oscillations in the shell will have a resonant frequencies between 700 and 800 Hz depending on how much of the shell participates in the oscillation. This brackets the observed spectral peak at 750-800 Hz. Coupled fluid-structure waves (Korteweg) will have a maximum resonant frequency of about 355 Hz. The sound speed in the water will decrease with increasing bubble volume so that when cavitation occurs, we expect lower phase speeds and frequencies than for single-phase water.

The vibrational mode responsible for the 1800-2300 Hz os-

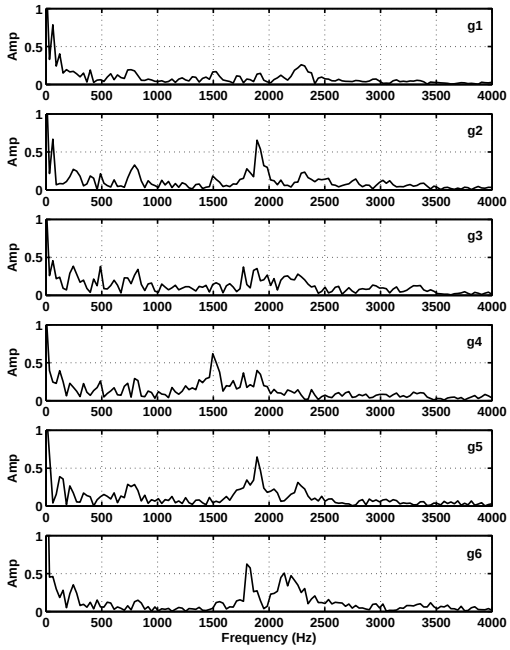

Figure 7. FFT analysis for data and time period shown in Fig. 6.

cillations is less obvious. One possibility is a circumferential mode of vibration induced by the off-axis impact of the projectile resulting in loading that is not coincident with the tube axis. Treating the tube as a circular ring, the vibration frequency is given by

$$f = \frac{1}{2\pi} \frac{n(n^2-1)}{\sqrt{n^2+1}} \sqrt{\frac{EI}{\rho AR^4}} \qquad (n = 2,3,...) \qquad (4)$$

where n indicates nth natural frequency, I is moment of inertia in tube cross section, A is area of tube cross section and R is radius of tube [17, 18]. The natural frequency of the mode n = 2 is calculated to be 2237 Hz, within the range (1800-2300 Hz) observed in the experiments.

Kinematic Analysis

After the projectile impact, the buffer was set into an oscillatory motion. Figure 8 shows the buffer and projectile motion after the impact as recorded by the high-speed camera. From the video we observed five distinct regimes of motion. Initially, the buffer was at a height 0 mm until the projectile impacted at $t = -0.68$ ms as seen in Fig. 8(a). At this time the buffer began to descend, compressing the water beneath it until $t = 2.86$ ms (Fig. 8(b)) when the buffer was observed to stop at a height of -9.5 mm. The buffer then began to ascend, lifting the projectile. The buffer and projectile separated at $t = 6.62$ ms (Fig. 8(c)) and height 6.6 mm, but the buffer continued to travel upwards where it reached a peak height of 18.1 mm at $t = 24.6$ ms (Fig. 8(d)). The buffer then gradually returned to its original location, stopping at 48.4 ms.

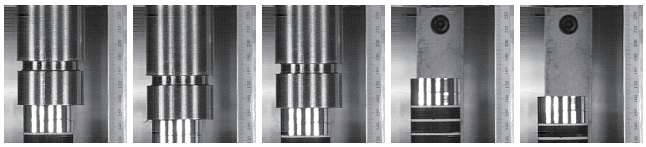

Figure 8. High-speed video images around the buffer and the projectile for shot 63 at (a) -0.68 ms, (b) 2.86 ms, (c) 6.62 ms, (d) 24.6 ms and (e) 48.4 ms.

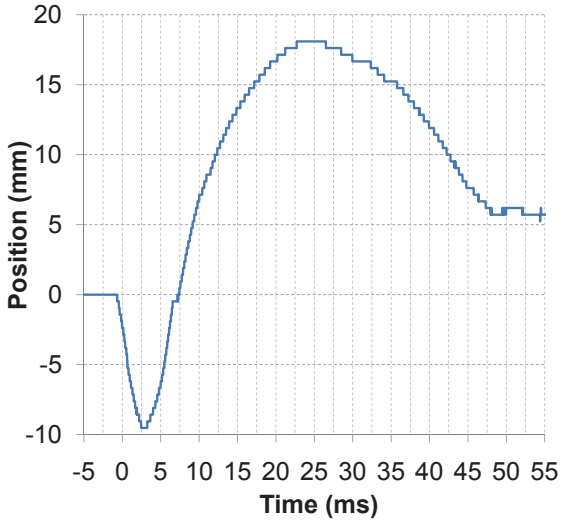

Figure 9. Top location history of the buffer obtained from the high-speed video images for shot 63.

The buffer is essentially rigid in these tests. This implies that the motion of the water immediately below the buffer may be inferred from the path of the top surface of the buffer. Therefore the buffer path as determined by the high-speed camera and shown in Fig. 9 depicts the motion of the top surface of the water. The projectile speed just before the impact and just after the detachment from the buffer was 6.2 m/s and 4.5 m/s, respectively. Using the projectile mass of 1.5 kg, the kinetic energy difference of the projectile before and after the impact is calculated as 13.6 J ($13.6\ \text{J} = 0.5 \times 1.5\ \text{kg} \times (6.2^2 - 4.5^2)\ \text{m}^2/\text{s}^2$). We suppose that most of this energy is transferred to the motion of the tube and water.

When the projectile impacts the top of the polycarbonate buffer, a stress wave propagates through the buffer, into the water column, and continues until it reaches the stationary bottom of the tube. A reflected wave is then created that propagates back through the water column and into the polycarbonate buffer. Further reflections will propagate down and up through the tube until they are eventually damped by viscosity. It takes 3.25 ms (0.44 ms through the buffer and 2.81 ms through the water) for the wave to complete the first round trip. This time corresponds to the times between Fig. 8(a) at -0.68 ms and Fig. 8(b) at 2.86 ms. It should be noted that upwards acceleration of the buffer was visible for times prior to 2.86 ms; 2.86 ms was the time when reverse (upwards) motion was first detected. Hence our data agrees with the relation between the wave propagation and buffer motion.

The detachment between the projectile and the buffer at 6.62 ms corresponds to the time at which the wave completes its second round trip. It was at this time that cavitation was first observed inside the tube as seen in Fig. 10. The presence of cavitation indicates that the pressure in the water has dropped below the vapor pressure of the water. The pressure will not decrease below the vapor pressure until all the water has evaporated. As this does not occur, we know that the pressure in the water is constant at the vapor pressure as long as cavitation is present. Thus the forces acting on the buffer are known and the buffer motion may be derived. The equation of motion balances the kinetic energy of the buffer just after the detachment (0.42 kg, 3.1 m/s) and the work by the differential force between the atmospheric pressure on the top surface (area = 1.12×10^{-3} m^2) and the vapor pressure on the bottom surface. At 298 K, the vapor pressure is 3.14 kPa [19]. Immediately after separation, the kinetic energy of the buffer was 2.02 J. This energy is approximately equal to the work done by the atmospheric pressure, 1.99 J. At the peak displacement of 18.1 mm (Fig. 8(d)), the potential energy of the buffer (0.07 J) was small and of the same order as the work done by the vapor pressure (0.06 J).

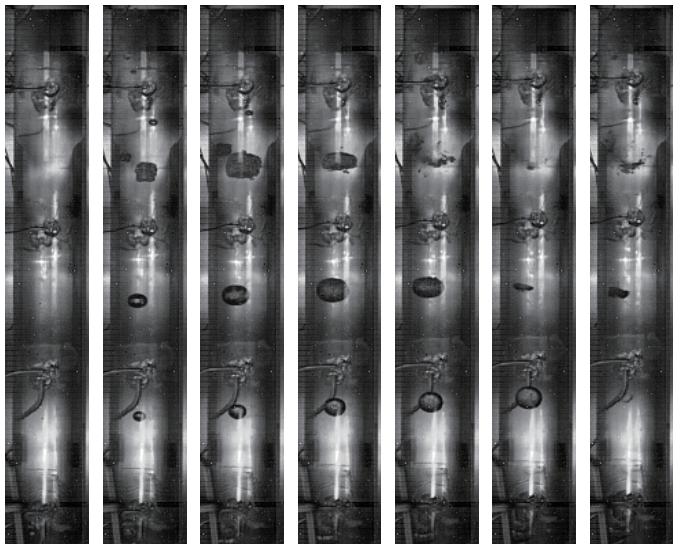

Figure 10. Series of frames from high-speed video showing the development and the collapse of cavitation bubbles around gages g3-g6 in shot 62. The top gage in the picture is g3. The first image is at $t = 8.1$ ms after trigger (8.78 ms after the projectile impact). The second image is at $t = 8.6$ ms and later images are at an interval of 1 ms.

In shot 62, the high-speed video camera captured the cavitation phenomena around gages g3-g6 (see Fig. 10). There are no bubbles in the first image of Fig. 10 at $t = 8.1$ ms but three big bubbles appear in the second image at 8.6 ms between gages g5-g6, g5-g4 and g4-g3. In addition to the big bubble between gages g4-g3, there are two more small bubbles in this vicinity. The sudden appearance of these bubbles is because the event occurs within 0.2 ms. Although the g5-g6 bubble becomes visible first, the size of the g4-g3 bubble is largest among them in the third frame when $t = 9.6$ ms. In the fourth frame of 10.6 ms, the g4-g3 bubble starts to collapse. The next several images portray the g5-g4 and g6-g5 bubbles collapse in turn as the wave propagates downward from g3 to g6. Since it takes about 3 ms to propagate from the g4-g3 bubble to the g6-g5 bubble (a distance of 0.2 m), the wave speed is approximately 66.7 m/s. The maximum void fraction due to cavitation is 2.32% as estimated by assuming the amount of cavitation is equal to the increase in water column volume as determined by the maximum height achieved by the buffer (18.1 mm). After cavitation occurs, the hoop strain

histories indicate that there was no significant expansion of the tube and hence the volume change due to the tube deformation may be neglected.

Cavitation Bubbles and Wave Propagation

Cavitation does not occur uniformly through the tube. As discussed by Wylie and Streeter [2], wave propagation changes the fluid velocity and head (pressure) so that the cavitation threshold depends on location. In this regard, our experiments are roughly similar to the situation of column separation with distributed vaporization in an upward-sloping pipe. The flow features in the present experiments are different at the initial stage than classical column separation due to the use of a piston rather than operating a valve to set up the wave motion. Another important difference is that the buffer motion can place the water column into tension.

On the middle part of the specimen tube, we observe discrete cavities (large cavitation bubbles) at several locations (see Fig. 10). Near the buffer bottom, cavitation bubbles were observed after the buffer rises past the original height. The duration of the cavitation bubbles near the top of the specimen was short, on the order of 0.5 ms, while the duration of the bubbles near the bottom end was long, on the order of 30-40 ms.

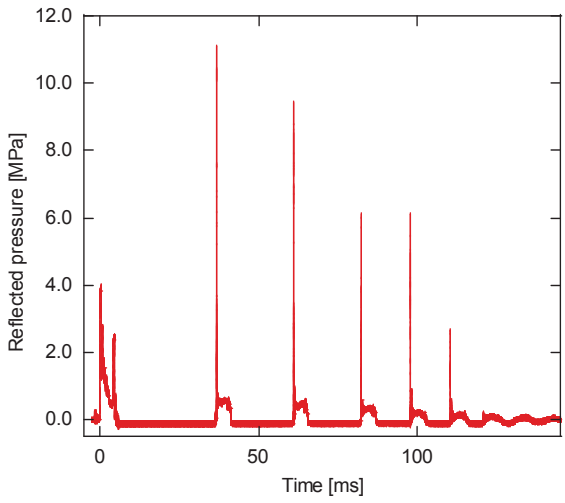

Figure 11. Reflected pressure history in shot 77 V_B=4.7 m/s, 3.1 mm thick-wall.

The reflected pressure history in shot 77 with tube #2 is shown in Fig. 11. The first and second peaks (2.6 and 6.8 ms after projectile impact) are caused by the initial impulsive loading and the reflected wave. About 30 ms after the second peak ($t = 38$ ms), there are a series of pressure spikes accompanied by a 4 to 5 ms pressure plateau. The duration of the plateau agrees with the reverberation time calculated with the Korteweg wave speed of 455 m/s. Since tube #2 has a thinner wall-thickness, the Korteweg speed is slower than that of tube #3. The top surface of the pressure transducer is 10 mm lower than the surroundings, which causes the extremely high pressure peaks of Fig. 11 when the cavitation bubbles collapse.

From analyzing the pressure signals and the high-speed movies, we conclude that the time between spikes in Fig. 11 is associated with several low speed waves propagating in the two-phase mixture or vaporous zone created by cavitation. For example, using the standard approximations for determining the sound speed in gas-liquid mixtures, we compute a speed of 90.5 m/s for a two-phase flow with 10% void fraction. The void fraction of 10% is the maximum fraction that would occur due to the observed volume associated with the buffer motion and the measured change in tube diameter during the experiment. The local void fraction could still be larger, but we expect the space-averaged volume fraction should be lower than 10% in our experiments.

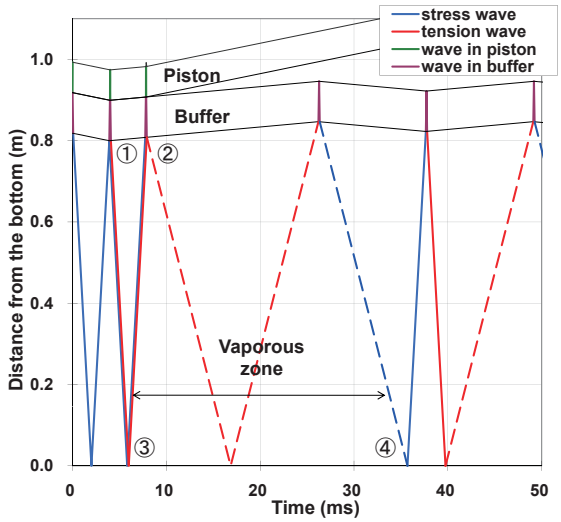

Figure 12. Schematic of waves, piston and buffer motion in cavitation events.

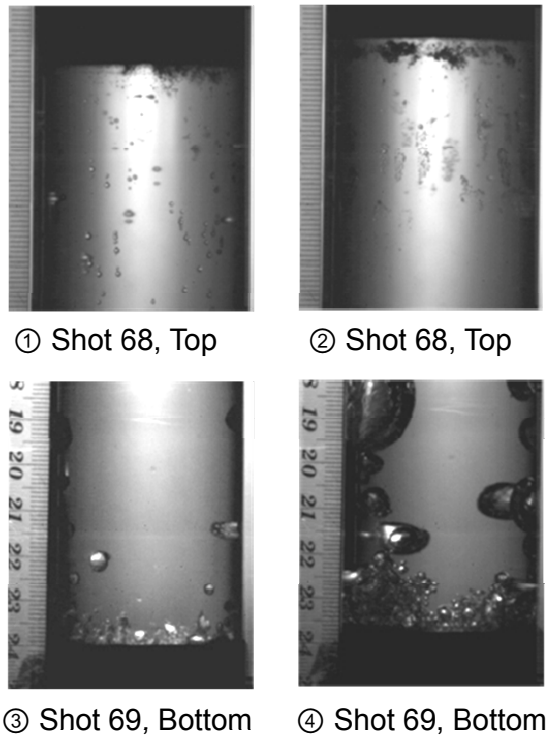

Figure 13. Cavitation bubbles in Shots 68 and 69. (Numbers correspond to the points indicated in Fig. 12).

The proposed wave propagation process is given in the $x-t$ diagram of Fig. 12. In this figure, the time of 0 ms is the instant of the piston impact. The images in Figure 13 are extracted from the movies in shots 68 and 69 and show flow features around the buffer bottom and the tube bottom such that the picture numbers 1 to 4 correspond to the points plotted in the $x-t$ diagram. From the movie, we see that the piston moves downward until 4 ms after impact and separates from the buffer at 7.4 ms. Instantaneous cavitation occurs below the buffer after the buffer and piston begins to move upward as shown in Fig. 13 (1). At the tube bottom, cavitation bubbles start to develop after the arrival of the first tension wave (3). The piston and the buffer separate from each other at 7.4 ms as indicated by rapid upward motion of the piston. After the separation, we observe a large number of instantaneous cavitation events (2). The first tension wave causes the reversal of the piston motion and the reflected (second) tension wave leads to the piston-buffer separation. The buffer upward motion stops at about 22 ms, reverses direction and stops again at about 41 ms. It is interesting to notice that the cavitation causes the bubbles to form structures reminiscent of grapes or a rosary.

Cavitation appears to occur throughout the water after the arrival of the second tension wave (2). The time between events (1) and (2) is close to the reverberation time calculated from the Korteweg speed without air entrainment. Although the details of wave propagation and the mixture condition are unknown, the subsequent buffer motion between events (2) and (4) is consistent with waves propagating through a vaporous zone. Cavitation is observed until the arrival of the compression wave (4) causes collapse of the vaporous zone. The pressure spikes of Fig. 11 appear to be associated with the collapse of the vapor bubbles and are very similar to those observed in shallow-water underwater explosion tests and simulations [20].

CONCLUSION

A steel projectile impacting a polycarbonate buffer was used to create stress and pressure waves that propagated through fluid-filled tubes. We observed the distinct sequence of downward wave propagation, reflection off the bottom plug, upward wave propagation, and reflection off the buffer for two complete cycles. The third cycle is visible, but considerably more vague than the first two cycles. During the third sequence, the pressure signal dropped to the vapor pressure of the water and cavitation events occurred. Several small, low-frequency peaks and high-frequency oscillations were observed in the hoop strain histories of the tube wall during the cavitation events. The low-frequency oscillations correspond to the forcing of the fluid-structure interaction and the high-frequency oscillations show agreement with the natural frequency of the circular ring which had the same dimensions and material properties of the tube. After the projectile impact, the buffer oscillated up and down. The buffer motion after the separation from the projectile was estimated by balancing the kinetic energy of the buffer just after the detachment and the work by the differential force between the atmospheric pressure and the vapor pressure.

Cavitation events occurred heterogeneously. At the top of the tube, instantaneous cavitation events occurred within 0.5 ms. The shape of the cavitation bubbles were round, but their assembly formed shapes resembling a bunch of grapes or a rosary. At the middle of the tube, the growth and collapse of several bubbles were observed over 3 ms. At the bottom of the tube, discrete cavity bubbles grew for a much longer period, about 30-40 ms.

ACKNOWLEDGMENT

This research was sponsored by the Office of Naval Research, DOD MURI on Mechanics and Mechanisms of Impulse Loading, Damage and Failure of Marine Structures and Materials (ONR Grant No. N00014-06-1-0730), program manager Dr. Y. D. S. Rajapakse. We thank Dr. Kikuo Kishimoto for fruitful discussion and Tim Curran for his work on data processing and image analysis.

REFERENCES

[1] Watters, G. Z., 1984. *Analysis and Control of Unsteady Flow in Pipelines*. Butterworth Publishers, MA.

[2] Wylie, E. B., and Streeter, V. L., 1993. *Fluid Transients in Systems*. Prentice-Hall, Inc., NJ.

[3] Wiggert, D. C., and Tijsseling, A. S., 2001. "Fluid transients and fluid-structure interaction in flexible liquid-filled piping". *Applied Mechanics Reviews,* **54**(5), pp. 455–481.

[4] Bergant, A., Simpson, A. R., and Tijsseling, A. S., 2006. "Water hammer with column separation: A historical review". *Journal of Fluids and Structures,* **22**, pp. 135–171.

[5] Fan, D., and Tijsseling, A. S., 1992. "Fluid-structure interaction with cavitation in transient pipe flows". *Transactions of the ASME,* **114**, pp. 268–273.

[6] Tijsseling, A. S., Vardy, A. E., and Fan, D., 1996. "Fluid-structure interaction and cavitation in a single-elbow pipe system". *Journal of Fluids and Structures,* **10**, pp. 395–420.

[7] Tijsseling, A. S., and Vardy, A. E., 2005. "Fluid-structure interaction and transient cavitation tests in a t-piece pipe". *Journal of Fluids and Structures,* **20**, pp. 753–762.

[8] Trevena, D., 1987. *Cavitation and Tension in Liquids*. Adam Hilger.

[9] Skews, B., Kosing, E., and Hattingh, R., 2004. "Use of a liquid shock tube as a device for the study of material deformation under impulsive loading conditions". *Proc. Instn. Mech. Engrs. J. Mechanical Engineering Science,* **218**, pp. 39–51.

[10] Espinosa, H., Lee, S., and Moldovan, N., 2006. "A novel fluid structure interaction experiment to investigate deformation of structural elements subjected to impulsive loading". *Experimental Mechanics,* **46**, p. 805824.

[11] Deshpande, V. S., Heaver, A., and Fleck, N. A., 2006. "An underwater shock simulator". *Proc. R. Soc. A,* **462**, pp. 1021–1041.

[12] Shepherd, J. E., and Inaba, K., 2010. "Shock loading and failure of fluid-filled tubular structures". In *Dynamic Failure of Materials and Structures*, A. Shukla, G. Ravichandran, and Y. Rajapakse, eds. Springer, pp. 153–190.

[13] Beltman, W. M., and Shepherd, J., 2002. "Linear elastic response of tubes to internal detonation loading". *Journal of Sound and Vibration,* **252**(4), pp. 617–655.

[14] Del Grosso, V., 1971. "Analysis of multimodel acoustic propagation in liquid cylinders with realistic boundary conditions - application to sound speed and absorption measurements". *Acustica,* **24**(6), pp. 299–311.

[15] Fuller, C. R., and Fahy, F. J., 1982. "Characteristics of wave propagation and energy distributions in cylindrical elastic shells filled with fluid". *J. Sound Vibration*, pp. 501–518.

[16] Lafleur, L., and Shields, F., 1995. "Low-frequency propagation modes in a liquid-filled elastic tube waveguide". *J. Acoust. Soc. Am.,* **97**(3), pp. 1435–1445.

[17] Hirashima, K., and Hirano, K., 1990. "Higher-order theories for free vibration analysis of circular rings". *Structural Eng./Earthquake Eng.,* **7**, pp. 189–192. Technical Note.

[18] Blevins, R. D., 1979. *Formulas for natural frequency and mode shape*. van Nostrand Reinhold Company.

[19] NAO, 2009. *Rika nenpyo (Chronological Scientific Tables)*. Maruzen Co., Ltd., Tokyo, JAPAN. National Astronomical Observatory.

[20] Wardlaw, A., and Ilamni, R., 2004. Simulation of underwater explosion cavitation phenomena. Tech. Rep. IHTR 2589, Indian Head Division, Naval Surface Warfare Center.